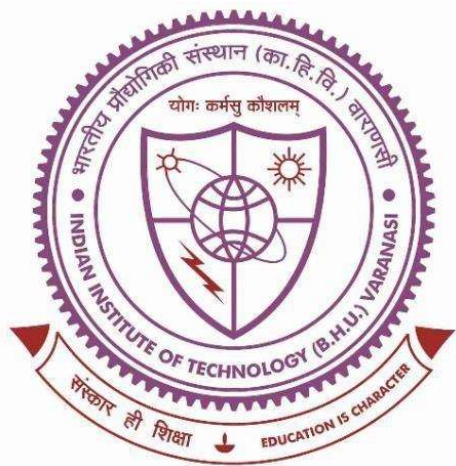


**Effect of processing routes on microstructure, phase evolution
and indentation characteristics of $\text{Fe}_{56.24}\text{Cr}_4\text{Mo}_{14}\text{C}_{15}\text{Si}_{3.8}\text{B}_6$,
 $\text{Fe}_{43.47}\text{Cr}_{15}\text{Mo}_{14}\text{C}_{15.12}\text{Si}_{3.78}\text{B}_6\text{Y}_2$, $\text{Fe}_{40.2}\text{Cr}_{20}\text{Mo}_{10}\text{W}_2\text{C}_{15}\text{Si}_{4.2}\text{B}_6\text{Y}_2$ and
 $\text{Fe}_{40.2}\text{Cr}_{15}\text{Mo}_{14}\text{Co}_3\text{C}_{15}\text{Si}_{4.2}\text{B}_6\text{Y}_2$ alloys**



THESIS SUBMITTED FOR THE DEGREE OF

DOCTOR OF PHILOSOPHY

IN

METALLURGICAL ENGINEERING

BY

SARIKA KUMARI

DEPARTMENT OF METALLURGICAL ENGINEERING

INDIAN INSTITUTE OF TECHNOLOGY

(BANARAS HINDU UNIVERSITY)

VARANASI – 221005

INDIA



भारतीय
प्रौद्योगिकी
संस्थान
काशी हिन्दू विश्वविद्यालय



INDIAN
INSTITUTE OF
TECHNOLOGY
BANARAS HINDU UNIVERSITY

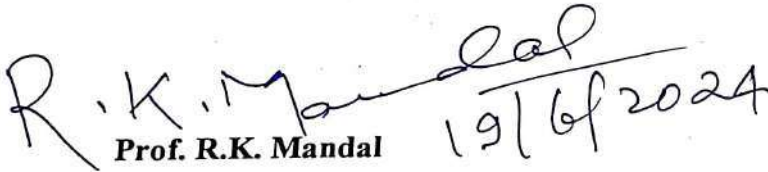
DEPARTMENT OF METALLURGICAL ENGINEERING

Indian Institute of Technology (BHU), Varanasi - 221005
Established by the Institutes of Technology (Amendment) Act, 2012 (No. 34 of 2012)

Phone : 0542-2307080-81, 2369346, Fax : 0542-2369478, email : head.met@iitbhu.ac.in

CERTIFICATE

It is certified that the work contained in the thesis entitled “Effect of processing routes on microstructure, phase evolution and indentation characteristics of $Fe_{56.24}Cr_4Mo_{14}C_{15}Si_{3.8}B_6$, $Fe_{43.47}Cr_{15}Mo_{14}C_{15.12}Si_{3.78}B_6Y_2$, $Fe_{40.2}Cr_{20}Mo_{10}W_2C_{15}Si_{4.2}B_6Y_2$ and $Fe_{40.2}Cr_{15}Mo_{14}Co_3C_{15}Si_{4.2}B_6Y_2$ alloys” by “Sarika Kumari” during this period she worked as a Ph.D. research scholar in this Department. The results and data presented in this thesis are genuine and original.


Prof. R.K. Mandal 19/6/2024

(Supervisor)

Department of Metallurgical Engineering

Indian Institute of Technology (BHU)
Varanasi-221005, Uttar Pradesh, India

Forwarded by:

(Prof. Sunil Mohan)

विभागाध्यक्ष / HEAD

धातुकीय अभियंत्रिकी विभाग

Department of Metallurgical Engg.

भारतीय प्रौद्योगिकी संस्थान (काशी हिन्दू विश्वविद्यालय)

Indian Institute of Technology (Banaras Hindu University)
Department of Metallurgical Engineering
Varanasi - 221005, Varanasi-221005

Indian Institute of Technology (BHU)

Varanasi – 221005, India

CANDIDATE'S DECLARATION

I, **Sarika Kumari**, certify that the work embodied in this Ph.D. thesis is my own bonafide work carried out by me under the supervision of **Prof. Rajiv Kumar Mandal** for a period of **July 2017 to June 2024** in the department of **Metallurgical Engineering IIT (BHU), Varanasi**. The matter embodied in this Ph.D. thesis has not been submitted for the award of any other degree/diploma.

I declare that I have devotedly acknowledged, given credit and referred to the research workers wherever their works have been cited in the text and the body of thesis. I further certify that I have not willfully copied some other's work, paragraph, text, data, as well as any results etc., reported in journals, books, magazines, reports dissertations, thesis, etc., or available at websites and have not included them in this thesis and have not cited as my own work.

Date: 19/6/2024

Place: Varanasi

A handwritten signature in black ink that reads "Sarika Kumari". The signature is written in a cursive style and is underlined with two parallel lines.

(Sarika Kumari)



भारतीय
प्रौद्योगिकी
संस्थान
काशी हिन्दू विश्वविद्यालय



INDIAN
INSTITUTE OF
TECHNOLOGY
BANARAS HINDU UNIVERSITY

DEPARTMENT OF METALLURGICAL ENGINEERING

Indian Institute of Technology (BHU), Varanasi - 221005

Established by the Institutes of Technology (Amendment) Act, 2012 (No. 34 of 2012)

Phone : 0542-2307080-81, 2369346, Fax : 0542-2369478, email : head.met@iitbhu.ac.in

UNDERTAKING BY THE CANDIDATE

I, **Sarika Kumari**, certify that the work carried out in the present thesis is my own work carried out by me under the supervision of **Prof. Rajiv Kumar Mandal** for the period from **July 2017 to June 2024** in the Department of Metallurgical Engineering IIT (BHU), Varanasi. The matter embodied in this thesis has not been submitted for the award of any degree/diploma.

(Sarika Kumari)



भारतीय
प्रौद्योगिकी
संस्थान
काशी हिन्दू विश्वविद्यालय



INDIAN
INSTITUTE OF
TECHNOLOGY
BANARAS HINDU UNIVERSITY

DEPARTMENT OF METALLURGICAL ENGINEERING

Indian Institute of Technology (BHU), Varanasi - 221005

Established by the Institutes of Technology (Amendment) Act, 2012 (No. 34 of 2012)

Phone : 0542-2307080-81, 2369346, Fax : 0542-2369478, email : head.met@iitbhu.ac.in

CERTIFICATE FROM THE SUPERVISORS

This is to certify that the above statement made by the candidate is correct to the best of our knowledge.

R.K. Mandal
19/6/2024

Prof. R.K. Mandal

(Supervisor)

Department of Metallurgical Engineering

Indian Institute of Technology (BHU)
Varanasi-221005, Uttar Pradesh, India

Forwarded by:

(Prof. Sunil Mohan)

विभागाध्यक्ष / HEAD

धातुकोय अभियंत्रिकी विभाग
Head of Department

Department of Metallurgical Engg.

भारतीय प्रौद्योगिकी संस्थान (काशी हिन्दू विश्वविद्यालय)

Indian Institute of Technology (Banaras Hindu University)
Department of Metallurgical Engineering
Varanasi - 221005 Varanasi-221005

Indian Institute of Technology (BHU)

Varanasi – 221005, UP, India



भारतीय
प्रौद्योगिकी
संस्थान
काशी हिन्दू विश्वविद्यालय



INDIAN
INSTITUTE OF
TECHNOLOGY
BANARAS HINDU UNIVERSITY

DEPARTMENT OF METALLURGICAL ENGINEERING

Indian Institute of Technology (BHU), Varanasi - 221005
Established by the Institutes of Technology (Amendment) Act. 2012 (No. 34 of 2012)

Phone : 0542-2307080-81, 2369346, Fax : 0542-2369478, email : head.met@iitbhu.ac.in

COURSE/ COMPREHENSIVE EXAMINATION/PRE-SUBMISSION SEMINAR COMPLETION CERTIFICATE

This is to certify that **Ms. Sarika Kumari**, a bonafide research scholar of this department, has satisfactorily completed the course work, comprehensive examination, and pre-submission seminar requirements, which are a part of her Ph.D. program.

Date: 19/06/2024

Place: Varanasi

Forwarded by:

(Prof. Sunil Mohan)
विभागाध्यक्ष / HEAD
धातुकीय अभियांत्रिकी विभाग
Department of Metallurgical Engg.
भारतीय प्रौद्योगिकी संस्थान (काशी हिन्दू विश्वविद्यालय)
Indian Institute of Technology (Banaras Hindu University)
Department of Metallurgical Engineering
221005 Varanasi-221005

Indian Institute of Technology (BHU)

Varanasi – 221005, UP, India



भारतीय
प्रौद्योगिकी
संस्थान
काशी हिन्दू विश्वविद्यालय



INDIAN
INSTITUTE OF
TECHNOLOGY
BANARAS HINDU UNIVERSITY

DEPARTMENT OF METALLURGICAL ENGINEERING

Indian Institute of Technology (BHU), Varanasi - 221005

Established by the Institutes of Technology (Amendment) Act. 2012 (No. 34 of 2012)

Phone : 0542-2307080-81, 2369346, Fax : 0542-2369478, email : head.met@iitbhu.ac.in

Date: 08.02.2024

Open Seminar Certificate

This is to certify that **Ms. Sarika Kumari** (Roll No. 17141010) D/o Shri Suman Prasad has delivered her Pre-Ph.D. seminar on **July 24, 2023 (Monday)** at 04:00 PM in the Department. The seminar was conducted under the Supervision of Prof. R. K. Mandal. She may be allowed to submit the Ph.D. thesis entitled "Effect of Processing Routes on Microstructure, Phase evolution and Indentation Characteristics of $Fe_{56.24}Cr_4Mo_{14}C_{15}Si_{3.8}B_6, Fe_{43.47}Cr_{15}Mo_{14}C_{15.12}Si_{3.78}B_6Y_2, Fe_{40.2}Cr_{20}Mo_{10}W_2C_{15}Si_{4.2}B_6Y_2$ and $Fe_{40.2}Cr_{15}Mo_{14}Co_3C_{15}Si_{4.2}B_6Y_2$ alloys".

(Sunil Mohan)

HEAD OF THE DEPARTMENT

धातुक्रीय अभियंत्रिकी विभाग

Department of Metallurgical Engg

भारतीय प्रौद्योगिकी संस्थान (काशी हिन्दू विश्वविद्यालय)

Indian Institute of Technology (Banaras Hindu University)

वाराणसी-221005/Varanasi-221005

20/2/24



भारतीय
प्रौद्योगिकी
संस्थान
काशी हिन्दू विश्वविद्यालय



INDIAN
INSTITUTE OF
TECHNOLOGY
BANARAS HINDU UNIVERSITY

DEPARTMENT OF METALLURGICAL ENGINEERING

Indian Institute of Technology (BHU), Varanasi - 221005

Established by the Institutes of Technology (Amendment) Act, 2012 (No. 34 of 2012)

Phone : 0542-2307080-81, 2369346, Fax : 0542-2369478, email : head.met@iitbhu.ac.in

COPYRIGHT TRANSFER CERTIFICATE

Title of Thesis: “Effect of processing routes on microstructure, phase evolution and indentation characteristics of $Fe_{56.24}Cr_4Mo_{14}C_{15}Si_{3.8}B_6$, $Fe_{43.47}Cr_{15}Mo_{14}C_{15.12}Si_{3.78}B_6Y_2$, $Fe_{40.2}Cr_{20}Mo_{10}W_2C_{15}Si_{4.2}B_6Y_2$ and $Fe_{40.2}Cr_{15}Mo_{14}Co_3C_{15}Si_{4.2}B_6Y_2$ alloys”

Candidate’s Name: Sarika Kumari

COPYRIGHT TRANSFER

The undersigned hereby assigns to the Indian Institute of Technology (BHU), Varanasi all rights under copyright that may exist in and for the above thesis submitted for the award of the Ph.D. degree.

Date: 19/06/2024

Place: Varanasi

(Sarika Kumari)

Acknowledgements

I would like to start with a thanking note to our GOD almighty for the wisdom he bestowed upon me, the strength and peace of mind in order to finish this research work. I was not alone in this journey; I received help from many hands to accomplish this incredible task. I am thankful to Indian Institute of Technology (BHU), Varanasi, for allowing me to pursue doctoral study.

I feel great pleasure in submitting my thesis. I express my deep sense of gratitude to my respected supervisor **Prof. Rajiv Kumar Mandal** for his patience and constant encouragements and support during all these years. I would like to acknowledge for his valuable suggestions which have always been a good source of inspiration and encouragement during my Ph.D. work.

I am extremely grateful to Prof. Sunil Mohan, Head of the Department of Metallurgical Engineering, IIT (BHU) for providing me the departmental facilities during my research period. I am also very much thankful to Prof. N. K. Mukhopadhyay, Dr. R. Manna, Dr. J. Basu, Prof. K. Chattopadhyay, Prof. B.N. Sarma, Dr. V. Jindal, Dr. A.K. Mondal and Dr. Sree H. Nandam for their fruitful discussions and help during my course work and research period.

I would like to express my gratitude to the entire non-teaching staff of the Metallurgical Engineering Department of IIT-BHU.

I would also like to acknowledge Prof. A.S.K Sinha RGIPT, Amethi, Uttar-Pradesh, India, for permitting us to carry out the SPS experiment, CSIR-NML Jharkhand India, for conducting a part of the melt-spinning experiments, AFMM, IISC Bangalore, for their support in TEM samples preparation and Central Instrument Facility of IIT-BHU. I would like to special thanks to Advanced Research Centre for Iron and steel of the institute funded by ministry of steel, government of India for providing high resolution diffractometer facility.

I would like to thanks to my seniors Dr. Manish Singh, Dr. Vikas Shivam, Dr. Vivek Pandey, Dr. Yagnesh Shadangi, Dr. Ankit Singh and Aman Kumar Lal Das for their valuable suggestions, co-operations and help at every stage of my research work. I am thankful to my classmates Dr. Nitesh, Dr. Shanker, Dr. Amit, Dr. Sandip, Mr. Roopchand, and Mr. Maanik for their appreciations and help during my Ph.D. work. My heartiest thanks to my friends (roommates) Dr. Dipti Tripathy, Dr. Pragya Shukla, Bhavna Srivastav and Urvashi for their

help, understanding and their cheerful company during this period. I am also very thankful to my juniors Harsh, Soham, Satyam, Priyosh, Rajat, Saptarishi and Sahil for their help and discussions.

I cannot conclude my acknowledgement without expressing my deep feelings for my family. My father (Late Mr Suman Prasad) is the person who has taken a step toward my higher study. He passed away during this journey, but his love and blessing are always with me. My elder sister Mrs Sunita and sister-in-law Mr. Shailendra Prasad are playing a significant role in my life, without their support and love I never reached here. I also would like to thank other family members Mr Bachchu Choudhary (father-in-law), Mr Chandan Kumar (brother), Dr. Ashmita Shah (niece), Sweta Shah (niece), Rishikesh Kumar (nephew), Dr. Harish Kumar for their consistency love, care and support. Words fail me to express my appreciation to my beloved husband Mr. Rakesh Ranjan and my little daughter Rishika Ranjan, who sacrificed a lot due to my research and give me pleasure in my life.

Especially thanks to my mother Mrs. Sereya Devi, for their unconditional love, support and care. She sacrifices a lot for me in her life till the end of my research day. I love you maa always.

Finally, I would like to thank everyone important to the fruitful realization of the thesis, as well as express my apology that I could not mention personally.

(Sarika Kumari)

Table of Contents

LIST OF ABBREVIATIONS	i
LIST OF SYMBOLS	ii
LIST OF FIGURES	iii
LIST OF TABLES	xii
PREFACE.....	xvi
Chapter 01: Introduction	1
1.1 Metallic Glass	1
1.2 Bulk Metallic Glasses.....	1
1.3 Concept of Glass Formation.....	2
1.4 Glass Forming Ability (GFA) and Glass Forming Criteria	5
1.5 Fabrication Technique and their Influences on Glass Formation and Properties.....	7
1.5.1 Preparation methods for Fe-based BMGs	7
1.5.2 Effects of Cooling rate on glass formation and properties	9
1.5.3 Effects of oxide impurities on glass formation and properties.....	10
1.6 Crystallization behaviour	13
1.6.1 Polymorphous Crystallization	13
1.6.2 Eutectic Crystallization	14
1.6.3 Primary Crystallization	15
1.7 Mechanical behaviour of MGs/BMGs.....	15
1.7.1 Plastic deformation	15
1.7.2 The free volume model	17
1.7.3 The Shear transformation zone (STZ) model.....	18
1.7.4 Shear bands in metallic glasses	19
1.7.5 Bulk metallic glass composites (BMGs composites).....	19
1.9 Applications	24
1.9.1 Soft magnetic materials	25
1.9.2 Structural materials.....	26
1.10 Objectives of the thesis	28
Chapter 02: Selection of Glass forming Fe-alloys based on empirical correlation	29
2.1 Introduction.....	30
2.2 Present Work.....	31
2.3 Computation of glass-forming parameters (e/a, V_R, R_R and K_F).....	33
2.4. The e/a, V_R, and R_R criteria for BMGs.....	35

2.5. Role of G_1 , G_2 , and K_F	39
2.6. Alloy Compositions Selection	41
2.7. Conclusions	42
Chapter 03: Materials and Experimental Details	43
3.1 Introduction	44
3.2 Materials Systems	44
3.3 Materials Synthesis Techniques	45
3.3.1 Cu-mould casting Technique	46
3.3.2 Melt-spinning Technique	47
3.3.3 High-Energy Ball milling Technique	49
3.3.4 Spark plasma sintering (SPS) Technique	51
3.3.5 Heat Treatment: Annealing Experiment	52
3.4 Techniques used for Characterization	53
3.4.1 Density Measurement	53
3.4.2 Optical Microscopy (OM): Microstructure Analysis	53
3.4.3 X-ray Diffraction (XRD) Technique: Structural and phase Analysis	53
3.4.5 Scanning Electron Microscopy (SEM): Morphology and Elemental mapping	54
3.4.6 Transmission Electron Microscopy (TEM): Microstructure and phase Analysis	55
3.4.7 Differential Scanning Calorimetry (DSC): Thermal Characterization	57
3.4.8 Indentation Characteristics: Mechanical property Measurements	58
Chapter 04: Copper-Mould Casting of Alloys	59
4.1 Introduction	59
4.2 Experimental Procedure	60
4.3 Results	61
4.3.1 Density Measurement	61
4.3.2 Evolution of Microstructures	62
4.3.3 Structural and Phase Characterization: X-ray diffraction	64
4.3.4 Thermal Analysis of as-cast alloys	70
4.3.5 Nature of Indentation of as-cast alloy at different loads	71
4.3.6 Determination of Indentation Fracture toughness (K_{IC})	76
4.3.7 Determination of Yield strength (σ_0), Meyer's exponent (n), material constant (K) ...	77
4.3.8 Determination of Plastic criterion (R_w), and Percentage of Elastic recovery (%R)	78
4.4 Discussions	81
4.4.1 Microstructure, Phase/Structure Analysis	81

4.4.2 Indentation Characteristics Analysis	82
4.5 Conclusions	84
Chapter-05: Melt-Spinning of Alloys	86
5.1 Introduction.....	86
5.2 Experimental Procedures	87
5.3 Results	89
5.3.1 Evolution of Microstructures	89
5.3.2 Structural and Phase Characterization: X-ray diffraction.....	90
5.3.3 Phase Analysis: Transmission Electron Microscopy (TEM).....	93
5.3.4 Morphology of melt-spun ribbon.....	96
5.3.5 Thermal behaviour Analysis	101
5.3.6 Nature of indentation of melt-spun ribbon at different load	102
5.3.7 Determination of Yield strength (σ_0), Meyer's exponent (n), material constant (K) .	107
5.3.8 Determination of Plastic criterion (R_w) and Percentage of Elastic recovery (%R)....	109
5.4 Discussion.....	111
5.4.1 Microstructure, Phase/Structure Analysis.....	111
5.4.2 Thermal Analysis	112
5.4.3 Indentation Characteristics Analysis	113
5.5 Conclusions	114
Chapter 06: Ball-Milling and Spark-Plasma Sintering of Alloys	115
6.1 Introduction.....	115
6.2 Experimental Procedure.....	116
6.3 Results	117
6.3.1 Density Measurement	117
6.3.2 Evolution of Microstructures	118
6.3.3 X-ray Diffraction Analysis of Ball milled Powder.....	119
6.3.4 X-ray Diffraction Analysis of SPSed alloys	124
6.3.5 Morphology of Ball milled Powder.....	127
6.3.6 Morphology of Sintered Alloy.....	129
6.3.7 Nature of Indentation of sintered alloys at different loads.....	137
6.3.8 Determination of Indentation Fracture toughness (K_{IC}).....	140
6.3.9 Determination of Yield strength (σ_0), Meyer's exponent (n), material constant (K) .	141
6.3.10 Determination of Plastic criterion (R_w) and Percentage of Elastic recovery (%R)..	143
6.4 Discussion.....	145

6.4.1 Microstructure, Phase/Structure Analysis.....	145
6.4.2 Indentation Characteristics Analysis	146
6.5 Conclusions	148
7.1 Summary.....	149
7.1.1 Synthesis and characterization of as-cast alloys.....	149
7.1.2 Glass/glass-nanocomposites formation in Fe-based alloys	150
7.1.3 Phase evolution and Indentation of Ball milled powder/ Pellets.....	150
7.2 Scope and suggestion for future work.....	151
ANNEXURE-I.....	152
References.....	162
List of Publications	199
List of Conferences/Workshops	200

LIST OF ABBREVIATIONS

MGs	Metallic glasses
BMGs	Bulk metallic glasses
ETMs	Early transition metals
TTT	Time-temperature-transformation
GFA	Glass forming ability
DRP	Dense random packing
ECP	Efficient cluster packing
RSP	Rapid solidification process
PBZ	Pseudo Brillouin zone
MA	Mechanical alloying
MM	Mechanical milling
SPS	Spark plasma sintering
SEM	Scanning electron microscopy
TEM	Transmission electron microscopy
RE	Rare earth element
DSC	Differential scanning calorimeter
DTA	Differential thermal analyser
STZ	Shear transformation zone
SLM	Selective laser melting
SAED	Selected area electron diffraction
HRTEM	High resolution transmission electron microscopy
SRO	Short-range order
MRO	Medium-range order
OM	Optical microscopy
XRD	X-ray diffraction
SE	Secondary electrons
EDAX	Energy Dispersive X-ray Spectroscopy
CI	Cast iron
PCA	Processing control reagent
WC	Tungsten carbide
BMP	Ball milled powder
PIPS	Precision ion polishing system
VHN	Vicker's hardness number
MS	Melt spinning
BF	Bright field
ISE	Indentation size effect
PM	Powder metallurgy
RISE	Reverse indentation size effect

LIST OF FIGURES

Fig. 1. 1: Variation of specific volume with temperature for a metal and glass-forming metals[15].	3
Fig. 1. 2: Schematic representation of T-T-T diagram during solid-liquid transformation[17]	4
Fig. 1. 3: Schematic representation of T-T-T diagram for pure metals, metallic-glass and bulk-metallic glass[17]	5
Fig. 1. 4: Schematic diagram of a new Cu-mould casting set-up invented by Gan et al.[53]...	8
Fig. 1. 5: A Schematic diagram of the J-quenching set-up[55].....	9
Fig. 1. 6: SEM images of indentation impression for different position, (a) edge, (b) middle, and (c) centre of $\text{Fe}_{36}\text{Co}_{36}\text{B}_{19}\text{Si}_5\text{Nb}_4$ BMG rods with diameter of 2mm under loading of 200g[70].....	11
Fig. 1. 7: SEM back-scattered image of the industrial grade Fe-Si alloy[71].....	11
Fig. 1. 8: Backscattered electron microprobe micrographs for the central part of 5mm drop-cast samples for the alloys (a) $\text{Fe}_{63}\text{Zr}_8\text{Co}_6\text{Al}_1\text{Mo}_7\text{B}_{15}$ and (b) $\text{Fe}_{60}\text{Zr}_{7.8}\text{Co}_6\text{Al}_1\text{Mo}_{6.9}\text{B}_{16.6}\text{Y}_{1.8}$ [76]	12
Fig. 1. 9: Hypothetical free energy vs. composition diagram for the Fe-rich, Fe-B alloy system[81].....	14
Fig. 1. 10: TEM images showing the microstructures obtained after (a) polymorphous crystallization, (b) eutectic crystallization, and (c) primary crystallization[81].....	15
Fig. 1. 11: Schematics representation of 2-D atomistic deformation mechanisms proposed for amorphous metals (a) the free volume model where diffusion like atomic jumps showing accommodation of strain[94] and (b) the shear transformation zone model where the entire cluster shear over the other to achieve a new configuration[101].	18
Fig. 1. 12: High magnification of a Zr-based BMG composite loaded in tension. The second phase promotes nucleation, multiplication and arrest of shear bands[109].	19

Fig. 1. 13: Different possibilities in in-situ composites (a) quasi-crystalline phase, (b) crystalline phase, (c) dendritic-crystalline phase and (d) two different amorphous phases[109].
.....20

Fig. 1. 14: SEM micrographs for alloy (a)Fe₃₀Co₂₁ (b) Fe₄₀Co₁₈ and (c)Fe₅₀Co₁₇ (d) HRTEM image and corresponding SAED patterns for the amorphous matrix in the Fe₄₀Co₁₈ alloy[110].
.....21

Fig. 1. 15: TEM images of SLM-fabricated Fe-based BMGCs with 40 vol.% Cu content: (a) Bright field TEM image, (b) (c) (d) HRTEM images and corresponding SAED patterns of the interface.....22

Fig. 1. 16: Relationship between coercivity and electrical resistivity for Fe- and Co-based glassy alloys[4].23

Fig. 1. 17: Licalloy powder core to power inductor in lap-top type personal computer[4]. .26

Fig. 1. 18: Schematic representation of Yield strength (Polymers, metals, composites and amorphous alloy) as a function of Young’s modulus[35].27

Fig. 1. 19: Tensile strength, Vickers hardness versus Young’s modulus for representative alloys in comparison with conventional crystalline alloys[19].28

Fig. 2. 1: A pie-chart graph representing number of metallic glasses (in %) based on different system 32

Fig. 2. 2: Venn diagram model (a) Fe-base system, (b) Cu-based system, (c) Zr-based system and (d) Ti-based system.36

Fig. 2. 3: Venn diagram model for (e) La-based system, (f) Co-based system.....37

Fig. 2. 4: Venn diagram model for (g) Al-based system, (h) Mg-based system, (i) Ni-based system and (j) Pd-based system.37

Fig. 3. 1: The Optical picture of Arc melting furnace unit with Cu-hearth.....	47
Fig. 3. 2: A schematic illustration of the melt-spinning technique	48
Fig. 3. 3: (a) Schematic representation of evolution of powder morphology and microstructures developed during MM/MA [149], (b) A Flow diagram represent various steps in MM process.	50
Fig. 3. 4 : (a) Schematic diagram of SEM, (b) Electron beam trajectory[151].....	55
Fig. 3. 5: (a) Schematic picture of a TEM Overall cabinet assembly; (b) inside view of a TEM[152]	56
Fig. 3. 6: A schematic diagram of trajectory of electron beam in diffraction mode and imaging mode.....	57
Fig. 4. 1: Optical image of (a) inside view of melting chamber, (b) Vacuum arc melting set-up, and (c) alloys buttons	60
Fig. 4. 2: Optical micrograph of master alloy (cast-iron), (a) without etched condition and (b) etched with 4% picral (vol. %) solution.....	62
Fig. 4. 3: (b) Optical micrograph from different region of Cu-mould cast alloy-A, etched with 5% nital, (a) Class 30 grey cast iron, ferrite dendrites and graphite in a ferrite matrix (ASM Metal handbook, Vol.9)[163].	63
Fig. 4. 4: (a-c) Optical micrograph of alloys-A, B, and C respectively, shows cementite matrix embedded with flaky (irregular dark colour) cementite and spheroidized (light grey colour dots) carbides: (d) microstructure of AISI 1074 steel, spheroidized carbides in ferrite matrix (ASM handbook, vol.9, page no.261)[163].	63
Fig. 4. 5: (a) X-ray diffraction pattern of as-cast alloy-A ($\text{Fe}_{56.24}\text{Cr}_4\text{Mo}_{14}\text{C}_{15}\text{Si}_{3.8}\text{B}_6$); (b) deconvolution of intense peaks.....	64
Fig. 4. 6: X-ray diffraction pattern of as-cast alloy-B ($\text{Fe}_{43.47}\text{Cr}_{15}\text{Mo}_{14}\text{C}_{15.12}\text{Si}_{3.78}\text{B}_6\text{Y}_2$).....	66

Fig. 4. 7: (a) X-ray diffraction pattern of as-cast alloy-B ($\text{Fe}_{40.2}\text{Cr}_{20}\text{Mo}_{10}\text{W}_2\text{C}_{15}\text{Si}_{4.2}\text{B}_6\text{Y}_2$) (b) deconvolution of intense peaks with a spread of 2θ of 41° - 46°	68
Fig. 4. 8: (a) X-ray diffraction pattern of as-cast alloy-B ($\text{Fe}_{40.2}\text{Cr}_{15}\text{Mo}_{14}\text{Co}_3\text{C}_{15}\text{Si}_{4.2}\text{B}_6\text{Y}_2$) (b) deconvolution of intense peaks with a spread of 2θ of 41° - 43°	69
Fig. 4. 9: DTA thermogram of Cu-mould cast alloys, (a) alloy-A, (b) alloy-B, (c) alloy-C, and (d) alloy-D, at constant heating rate of $20^\circ\text{C}/\text{min}$	71
Fig. 4. 10: Optical images of Vickers micro-indentation impressions of master alloy (cast iron) at various loads, showing crack free up to 1000g indentation load	72
Fig. 4. 11: Optical images of indentation impression from various region for Cu-mould cast alloys (a) alloy-A, (b) alloy-B, (c) alloy-C, and (d) alloy-D, showing nature of indentation with load up to fracture	72
Fig. 4. 12: Shows nature of variation of indentation size with load in (a) alloy A, (b) alloy B, (c) alloy C, and (d) alloy D	73
Fig. 4. 13: Variation of hardness (VHN) with respect to load (g) for master alloy (grey cast iron).....	74
Fig. 4. 14: Variation of hardness (VHN) with respect to load (g) for the Cu-mould cast alloys (a) alloy-A, (b) alloy-B, (c) alloy-C, and (d) alloy-D (arrows marks showing cracks occurs at that load)	75
Fig. 4. 15: Optical micrographs showing indentation impression with radial crack on (a) alloy-B and (b) alloy-D at a 1000g load.....	76
Fig. 4. 16: Log P vs Log d plots for Cu-mould cast alloys (a) alloy-A, (b) alloy-B, (c) alloy-C and (d) alloy-D. The lines are the linear fit to the data and R^2 is the correlation coefficient and having values ~ 0.99	77

Fig. 4. 17: (a) Comparison of hardness (VHN) at indentation load of 100g among all alloys processed through Cu-mould casting and (b) Load-displacement (P-h plot) response of as-cast alloys at 100g indentation load 78

Fig. 4. 18: P-h curve for loading and unloading, and their associated nomenclature[174]..... 79

Fig. 5. 1: Macroscopic images of melt-spun ribbons. 88

Fig. 5. 2: Optical image of melt-spun ribbon in etched condition (a) MS-A, (b) MS-B, (c) MS-C and (d) MS-D. 90

Fig. 5. 3: XRD pattern of melt-spun ribbons (a) as-synthesized MS-A, (b) annealed MS-A (at 908K for 1h), (C) as-synthesized MS-B and (d) annealed MS-B (at 908K for 1h)..... 91

Fig. 5. 4: XRD pattern of melt-spun ribbon MS-C; (a) as-synthesized at different speed and (b) annealed ribbon (at 918K for 1h)..... 92

Fig. 5. 5: XRD pattern of melt-spun ribbon MS-D; (a) as-synthesized at different speed and (b) annealed ribbon (at 918K for 1h)..... 93

Fig. 5. 6: (a) and (c) Bright field (BF) image of melt-spun ribbons MS-A and MS-D with (b) and (d) corresponding diffraction patterns showing diffuse halos..... 93

Fig. 5. 7: (a) Bright field image of MS-B sample and inset shows corresponding diffraction pattern, (b) bright field image of same sample from different place and (c) corresponding inverted diffraction pattern superimposed with actual diffraction pattern. 1→Fe₁₁Mo₆C₅; 2→α-Fe..... 94

Fig. 5. 8: (a) Bright field image of MS-C sample and inset shows corresponding diffraction pattern (b) bright field image from different place of same sample and (c) corresponding inverted diffraction pattern superimposed with actual diffraction pattern: 1→Fe₁₁Mo₆C₅..... 95

Fig. 5. 9: (a-c) SEM images of MS-A sample at same magnification, showing full area, spot 1, and spot 2; (d-f) Energy dispersive spectra (EDS) of the marked area. 96

Fig. 5. 10: (a-c) SEM images of MS-B sample at same magnification, showing full area, spot 1, and spot 2; (d-f) EDS spectrum of the marked area.....	97
Fig. 5. 11: (a-c) SEM images of MS-C sample at same magnification, showing full area, spot 1, and spot 2; (d-f) EDS spectrum of the marked area.....	99
Fig. 5. 12: (a-c) SEM images of MS-D sample at same magnification, showing full area, spot 1, and spot 2; (d-f) EDS spectrum of the marked area.....	100
Fig. 5. 13: DTA thermogram of melt-spun ribbons, (a) MS-A, and (b) MS-C, with heating rate of 20°C/min.....	102
Fig. 5. 14: Optical images of indentation impression from various region for as-synthesized ribbons (a) MS-A, (b) MS-B, (c) MS-C, and (d) MS-D, showing nature of indentation with load up to fracture. Shear bands are formed around the indentation periphery and cracks are also observed.....	103
Fig. 5. 15: Shows nature of variation of indentation size with load in (a) MS-A, (b) MS-B, (c) MS-C, and (d) MS-D.	103
Fig. 5. 16: Variation of hardness (VHN) with respect to load (g) for the melt-spun ribbons ribbon and annealed ribbons of (a) MS-A, (b) MS-B, (c) MS-C, and (d) MS-D.	104
Fig. 5. 17: Dependence of the indentation hardness on depth (maximum) for melt-spun ribbons (MS) and annealed ribbons (AMS).....	106
Fig. 5. 18: Comparison of hardness (GPa) at indentation load of 75g among all the melt-spun ribbons (as-synthesized) and annealed ribbons.....	107
Fig. 5. 19: Log P vs Log d plots for melt-spun ribbon samples, (a) MS-A, (b) MS-B, (c) MS-C, and (d) MS-D. The lines are the linear fit to the data and R^2 is the correlation coefficient and having value in the range 0.92-0.99.....	108
Fig. 5. 20: Load-displacement (P-h) plot of (a) melt-spun ribbons and (b) annealed ribbons (AMS) at 75g load.	109

Fig. 6. 1: Optical image of SPSed samples with 10mm diameter disc.....	116
Fig. 6. 2: Showing optical micrographs of 100h ball milled powders of sintered samples (a) SPSed-A, (b) SPSed-B, (c) SPSed-C, and (d) SPSed-D, sintered at 800 °C.	118
Fig. 6. 3: Showing SEM images of 100h ball milled powders of sintered samples (a) SPSed-A, (b) SPSed-B, (c) SPSed-C, and (d) SPSed-D, sintered at 800 °C.....	119
Fig. 6. 4: X-ray diffraction patterns of ball-milled sample BMP-A ($\text{Fe}_{56.24}\text{Cr}_4\text{Mo}_{14}\text{C}_{15}\text{Si}_{3.8}\text{B}_6$), at various milling time	120
Fig. 6. 5: X-ray diffraction patterns of ball-milled BMP-B ($\text{Fe}_{43.47}\text{Cr}_{15}\text{Mo}_{14}\text{C}_{15.12}\text{Si}_{3.78}\text{B}_6\text{Y}_2$) sample, at various milling time.....	121
Fig. 6. 6: X-ray diffraction patterns of ball-milled BMP-C ($\text{Fe}_{40.2}\text{Cr}_{20}\text{Mo}_{10}\text{W}_2\text{C}_{15}\text{Si}_{4.2}\text{B}_6\text{Y}_2$) sample, at various milling time.....	121
Fig. 6. 7: X-ray diffraction patterns of ball-milled BMP-D ($\text{Fe}_{40.2}\text{Cr}_{15}\text{Mo}_{14}\text{Co}_3\text{C}_{15}\text{Si}_{4.2}\text{B}_6\text{Y}_2$) sample, at various milling time.....	122
Fig. 6. 8: Variation of average crystallite-size and micro-strain with milling time of ball-milled powders (a) BMP-A, (b) BMP-B, (c) BMP-C, and (d) BMP-D.....	123
Fig. 6. 9: X-ray diffraction patterns of composition-A, (i) 100h ball-milled nanocomposite powder and (ii) sintered composite at 800°C.....	124
Fig. 6. 10: X-ray diffraction patterns of composition-B, (i) 100h ball-milled nanocomposite powder and (ii) sintered composite sample.	125
Fig. 6. 11: X-ray diffraction patterns of composition-C, (i) 100h ball-milled nanocomposite powder and (ii) sintered sample.....	125
Fig. 6. 12: X-ray diffraction patterns of composition-D, (i) 100h ball-milled nanocomposite powder and (ii) sintered composite sample.	126

Fig. 6. 13: (a-c) shows SEM micrograph of powders of (A) BMP-A, and (B) BMP-B with different milling time and the histogram shown in (d-f) depicts their particle size distribution. 128

Fig. 6. 14: (a-c) shows SEM micrograph of powders of (C) BMP-C, and (D) BMP-D with different milling time and the histogram shown in (d-f) depicts their particle size distribution. 128

Fig. 6. 15: SEM micrograph of SPSed-A (a) spark plasma sintered at 800 °C and showing selected area for elemental mapping; (b) distribution of all the elements within the selected area; (c) SEM-EDS chemical composition of individual elements corresponding to the selected area; (d-j) individual elemental distribution within the selected area. 129

Fig. 6. 16: (a-c) SEM images of SPSed-A sample at same magnification, showing full area, spot 1, and spot 2; (d-f) EDS spectrum of the marked area. 130

Fig. 6. 17: SEM micrograph of SPSed-B (a) spark plasma sintered at 800 °C and showing selected area for elemental mapping; (b) distribution of all the elements within the selected area; (c) SEM-EDS chemical composition of individual elements corresponding to the selected area; (d-k) individual elemental distribution within the selected area. 131

Fig. 6. 18: (a-c) SEM images of SPSed-B sample at same magnification, showing full area, spot 1, and spot 2; (d-f) EDS spectrum of the marked area. 132

Fig. 6. 19: SEM micrograph of SPSed-C (a) spark plasma sintered at 800 °C and showing selected area for elemental mapping; (b) distribution of all the elements within the selected area; (c) SEM-EDS chemical composition of individual elements corresponding to the selected area; (d-k) individual elemental distribution within the selected area. 133

Fig. 6. 20: (a-c) SEM images of SPSed-C sample at same magnification, showing full area, spot 1, and spot 2; (d-f) EDS spectrum of the marked area. 134

Fig. 6. 21: SEM micrograph of SPSed-D (a) spark plasma sintered at 800 °C and showing selected area for elemental mapping; (b) distribution of all the elements within the selected area; (c) SEM-EDS chemical composition of individual elements corresponding to the selected area; (d-l) individual elemental distribution within the selected area.....	135
Fig. 6. 22: (a-c) SEM images of SPSed-D sample at same magnification, showing full area, spot 1, and spot 2; (d-f) EDS spectrum of the marked area.....	136
Fig. 6. 23: Optical images of indentation impression from various region for sintered alloys (a) SPSed-B, (b) SPSed-C, and (c) SPSed-D, showing nature of indentation with load up to fracture.....	137
Fig. 6. 24: Shows nature of variation of indentation size with load in (a) SPSed-A, (b) SPSed-B, (c) SPSed-C, and (d) SPSed-D.....	138
Fig. 6. 25: Variation of hardness (GPa) with respect to load (mN) for the SPSed alloys (a) SPSed-A, (b) SPSed-B, (c) SPSed-C, and (d) SPSed-D.....	139
Fig. 6. 26: SEM micrographs showing indentation impression at 1000g load (a) SPSed-A, (b) SPSed-B, (c) SPSed-C, and (d) SPSed-D. The arrow marks showing radial cracks.....	140
Fig. 6. 27: Log P vs Log d plots for sintered composite, (a) SPSed-A, (b) SPSed-B, (c) SPSed-C, and (d) SPSed-D. The lines are the linear fit to the data and R^2 is the correlation coefficient and having value in the range 0.96-0.99.....	142
Fig. 6. 28: (a) Comparison of hardness (VHN) at indentation load of 100g among all sintered composites; (b) Load-displacement (p-h) plot response of sintered composite at 100g load; (c) showing pop-in marks in unloading (P-h) curve.....	143

LIST OF SYMBOLS

T_g	glass transition temperature
T_m	melting temperature
R_c	critical cooling rate
T_N	nose temperature
T_l	liquidus temperature
t_N	time required for the nucleation of the first crystallite
D_c	critical thickness
e/a	electron to atom ratio
V_R	volume ratio
R_R	radius ratio/ atomic size ratio
K_F	Fermi wave vector
T_{rg}	reduced glass transition temperature
ΔT	undercooled liquid regime
T_x	crystallization temperature
ΔG_m	activation energy of motion
Ω	atomic volume
ν	Poisson's ratio
γ_0	Shear strain
ε	dilatational strain
H_v	Vicker's hardness
G	radius of pseudo-Brillouin zone surface
λ	wave length
t	crystallite size
β	total broadening
θ	Bragg angle
ρ	bulk density
P	load
d	indentation diagonal length
K_{IC}	indentation fracture toughness
E	Young's modulus
σ_0	offset yield strength
n	Meyer's exponent
K	material constant
W_e	plastic work
W_p	elastic work
R	elastic recovery
h_f	final depth of the indentation
h_{max}	maximum penetration depth
R_w	plastic criterion

LIST OF TABLES

Table 1. 1: Fe-based BMG alloy system reported together with the calendar years	2
Table1.2: Some Fe-based alloys and their applications.....	24-25
Table 2. 1: Type of metallic glasses based on different system.....	32
Table 2. 2: State of Valence(s) of various Elements.....	33
Table 2. 3: Value of atomic radius in (A°) of various elements.....	34
Table 2. 4: Number of systems following glass forming criteria in the range given in columns 5 to 7.....	37
Table 2. 5: Number of alloy systems falling in the intersection regions of the Venn diagrams.....	38
Table 2. 6: Crystallographic details of phases after devitrification or crystallization of BMGs	41
Table 2. 7: Selected Compositions with various glass-forming parameters (based on Venn diagram model)	42
Table 3. 1: The master alloy composition and nominal compositions with various parameters	45
Table 3. 2: Physical properties of elements used for synthesis of alloys, composites, and amorphous alloys.	45
Table 3. 3: Detail information regarding ball-milling nanocomposite powders.....	51

Table 3. 4: Processing parameters for compaction of ball-milled powder composite by SPS technique.....	52
Table 4. 1: The bulk (experimental) density of Cu-mould cast alloy	61
Table 4. 2: The d-spacing values corresponding to their (hkl) planes of the observed phases in Alloy-A	65
Table 4. 3: The d-spacing values corresponding to their (hkl) planes of the observed phases in Alloy-B	67
Table 4. 4: The d-spacing values corresponding to their (hkl) planes of the observed phases in Alloy-C	68
Table 4. 5: The d-spacing values corresponding to their (hkl) planes of the observed phases in Alloy-D	69
Table 4. 6: Phases recognised after deconvolution of peaks.....	70
Table 4. 7: Indentation diagonal length, microhardness data in GPa at various.....	75
Table 4. 8: Fracture toughness of Cu-mould cast alloys at a load of 1000g.....	76
Table 4. 9: Values of average VHN, E, n, Log K, and σ_0 of as-cast alloys at 100g load	78
Table 4. 10: The Mechanical properties of the tested alloys estimated from P-h plot at 100g indentation load.....	80
Table 4. 11: Some important Mechanical properties of Cu-mould cast alloys at 100g load..	80
Table 4. 12: Detail information of the phases evolved in the alloys processed through Cu-mould casting	82
Table 5. 1: Specifications of melt-spinner and melt-spun ribbons.	87
Table 5. 2: Elemental composition of MS-A sample by point EDS analysis.	97
Table 5. 3: Elemental composition of MS-B sample by point EDS analysis.	98

Table 5. 4: Elemental composition of MS-C sample by point EDS analysis	99
Table 5. 5: Elemental composition of MS-D sample by point EDS analysis.	101
Table 5. 6: Thermal parameters by DTA scan of melt-spun ribbon samples at heating rate of 20 °C/min. (all temperatures are in °C).....	102
Table 5. 7: Microhardness data in GPa at various loads for melt-spun ribbons and annealed sample (AMS) are displayed. Latter is indicated in bold face.....	105
Table 5. 8: Values of average VHN, E, n, Log K, and σ_0 of melt spun ribbons at 75g load.	108
Table 5. 9: The Mechanical properties of the tested melt-spun ribbons estimated from P-h plot at 75g indentation load.....	110
Table 5. 10: The Mechanical properties of the tested annealed melt-spun ribbons estimated from P-h plot at 75g indentation load.	110
Table 5. 11: Some important Mechanical properties of melt-spun ribbons and annealed ribbons at 75g load.....	111
Table 6. 1: The bulk (experimental) density of Sintered composite.....	117
Table 6. 2: Variation of average crystallite size and micro-strain with milling time in ball-milled nanocomposite powder	123
Table 6. 3: Detail information of the phases evolved in the sintered samples.....	127
Table 6. 4: Variation of particle size (in μm) with milling time in ball-milled Powder samples	129
Table 6. 5: Elemental composition of SPSed-A sample by point EDS analysis.	130
Table 6. 6: Elemental composition of SPSed-B sample by point EDS analysis.....	132
Table 6. 7: Elemental composition of SPSed-C sample by point EDS analysis.....	134
Table 6. 8: Elemental composition of SPSed-C sample by point EDS analysis.....	136

Table 6. 9: Indentation diagonal length, microhardness data in GPa at various.....	140
Table 6. 10: Fracture toughness of sintered composites at 1000g indentation load.	141
Table 6. 11: Values of average VHN, E, n, Log K, and σ_0 of Sintered alloy at 100g load ..	143
Table 6. 12: The Mechanical properties of the tested sintered alloy estimated from P-h plot at 100g indentation load.....	144
Table 6. 13: Some important Mechanical properties of SPSed alloy at 100g load.....	145

PREFACE

Kelton (2023) has recently commented, “Metallic glasses have the potential to become transformative materials, but this is hindered by the lack of ability to accurately predict which metallic alloys will form good glasses. Current approaches are limited to empirical rules that often rely on parameters that are unknown until the glasses are made, rendering them not predictive”. The research work carried out as a part of this doctoral thesis shall revolve around such a hypothesis. The thesis has two distinct parts. One of them relates to evolving parameters of metallic systems for empirically predicting metallic glass compositions. These parameters are: electron to atom ratio (e/a), Volume ratio of total volume per mole of the alloy to largest atom volume (V_R), and radius ratio of the larger atom to smaller atom in alloy (R_R). In addition to these, the concept of Fermi energy (E_F) and Fermi vector (K_F) will also be computed. Further the interaction of Fermi surface with that of Pseudo-Brillouin Zone (PBZ) boundary has also been explored. Based on these considerations four iron based alloy compositions have been chosen for experimental investigations. The thesis has been organised in seven chapters and one appendix.

Chapter 1 gives brief introduction of various reports by researchers on metallic glasses (MGs) and bulk metallic glasses (BMGs). The historical background of MGs shall begin with first report by Pol Duwez (1960) followed by seminal contributions made by T.R. Ananthraman from this department. Majority of MGs compositions investigated since their inception refer to exploring the properties related to transformer core application as soft magnetic material. Such MGs was having iron as the main alloying element. It has recently been shown that Fe-based MGs compositions can also be useful for structural application. Several researchers compared hardness to density ratio (H/ρ) of Fe-based BMGs with that of maraging steel. They have concluded such a ratio for BMGs is around four times more than maraging steel. This investigation has kept in mind this aspect while choosing four compositions based on the empirical criteria studied for around 1000 alloys. A series of Venn diagrams were constructed for each of the categories of metallic alloys for MGs/BMGs. The thesis will present the detail computational steps for all of them. The data utilised for this purpose will be given as an Annexure-I. Essential steps pertaining to these will be explained in (**chapter 2**). The four compositions chosen as a part of this investigation along with relevant empirical parameters will be given at the end of this chapter as a part of conclusion. This chapter will emphasize only details of MGs/BMGs compositions with iron as a main alloying element for the reasons

explained above. The alloy compositions selected as a part of this investigation has been synthesized by Cu-mould casting. Such a synthesized alloy will be designated as Cu-mould cast alloy in the thesis.

Chapter 3 deals with experimental part along with details of raw materials utilized for alloy making. These four alloys were subjected to further processing. The processing methods relate to (i) melt-spinning and (ii) high energy ball-milling followed by compaction through spark plasma sintering (SPS). The characterization tools employed for Cu-mould cast, melt-spun ribbons, ball-milled powders as well as their compact will be briefly discussed in this chapter. They refer to optical and electron microscopy. Extensive uses of X-ray diffraction (Rigaku Miniflex 600, EMPYREAN PANALYTICAL HR-XRD) have been done. Melt-spun ribbons were examined under transmission electron microscope in diffraction and imaging modes for conformation of glassy nature. The hardness of samples of as-cast alloy as well as after processing was measured through instrumented hardness tester (make: Anton Paar MHT³). The stability of the alloys under processing different processing conditions was studied with the help of DTA (make: NETZSCH DSC 404F3).

Chapter 4 begins with discussion on the evolution of structures/microstructures of Cu-mould cast alloys. The phases evolved in these alloys were having structure hP20, oP40, mC28, cF112, cI58, cF116, and oP16 type. Most of the phases are common in them. Alloy-A has shown dendritic features in their microstructure. Alloy-D exhibits minimum density (7.23g/cc) and maximum melting temperature (1418K) among all. This chapter also deals with relation of hardness with alloying additions. Alloy-D (3 at% addition of Co) exhibits maximum microhardness (~13 GPa) and Young's modulus value (~240GPa) at 100g indentation load. The hardness to density ratio for all as-cast alloys are higher than maraging steel.

Chapter 5 deals with synthesis, characterization, thermal stability and indentation behaviour of melt-spun ribbons. Alloy compositions A and D in ribbon form exhibits X-ray amorphous structures. Transmission electron microscopy (TEM) observations confirm that ribbon MS-A and MS-D are indeed amorphous. In contrast MS-B and MS-C consist of very fine nanocrystalline phases are distributed in the amorphous matrix. These nanocrystals are one of the two phases or both (α -Fe and Fe₁₁Mo₆C₅ phases). Melt-spun ribbon MS-D also exhibits maximum melting temperature (1433K). Melt-spun ribbons MS-A and MS-C have clear glass transition temperature at T_g 923K and 882K respectively. The reduced glass transition temperatures Trg of these ribbons are found to be 0.55 and 0.53 respectively.

The next synthesis method, I have used high energy ball milling technique. This is discussed in **chapter 6**. As-cast alloys when processed through high energy ball milling retain only two phases at the end of 100h of milling. They are α -Fe and $\text{Fe}_{11}\text{Mo}_6\text{C}_5$ phase. These phases are present under all processing conditions. The average crystallite size and average strain were calculated. Further, 100h ball-milled powders were consolidated through SPS technique. Spark plasma sintered samples (SPSed) give rise to additional crystalline phases Fe_{23}C_6 (cF116) and FeMoB_2 (tP10). Phase transformation takes place during the process of SPS in addition to consolidation. The densities of sintered powder samples are same as those of as-cast sample except SPSed-A and SPSed-D. The hardness to density ratio of SPSed alloys are also better than maraging steel.

Chapter 7 summarizes the outcome of entire work. It also has a section on the scope of future work.